Journal of Colloid and Interface Science 648 (2023) 488–496

Contents lists available at ScienceDirect

Journal of Colloid And Interface Science

journal homepage: www.elsevier.com/locate/jcis

Fusogenic Cell-Derived nanocarriers for cytosolic delivery of cargo inside living cells

Enrica Soprano, Martina Migliavacca, Miriam López-Ferreiro, Beatriz Pelaz, Ester Polo *, Pablo del Pino *

Centro Singular de Investigación en Química Biolóxica e Materiais Moleculares (CiQUS), Universidade de Santiago de Compostela. Rúa Jenaro de la Fuente s/n, 15705 Santiago de Compostela Spain

GRAPHICAL ABSTRACT

Fusogenic cancer cell-derived nanocarriers, combining homotypic targeting capabilities and fusogenic properties, are capable of fast intracellular delivery of the encapsulated payloads into the cytosol of living cells.

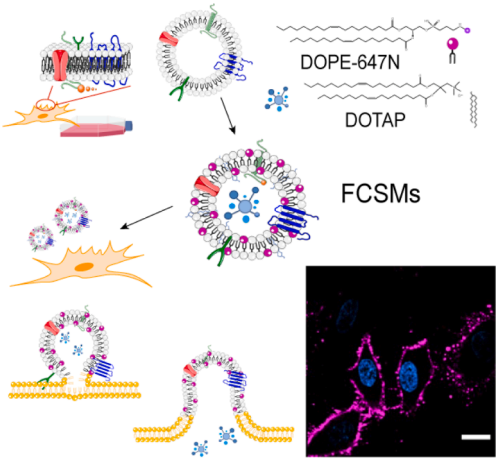

ARTICLE INFO

Keywords:
Biomimetic
Intracellular delivery
Nanocarrier
Fusogenic
Cell membrane coating

ABSTRACT

A surface-engineered cell-derived nanocarrier was developed for efficient cytosolic delivery of encapsulated biologically active molecules inside living cells. Thus, a combination of aromatic-labeled and cationic lipids, instrumental in providing fusogenic properties, was intercalated into the biomimetic shell of self-assembled nanocarriers formed from cell membrane extracts. The nanocarriers were loaded, as a proof of concept, with either bisbenzimide molecules, a fluorescently labeled dextran polymer, the bicyclic heptapeptide phalloidin, fluorescently labeled polystyrene nanoparticles or a ribonucleoprotein complex (Cas9/sgRNA). The

Abbreviations: Cas9, CRISPR-associated protein 9; CSM, cellsome; FCSM, fusogenic cellsome; CTCF, corrected total cell fluorescence; DLS, dynamic light scattering; DS, dextran-snarf; EM, electron microscopy; HOE, Hoechst H 33,258; MFI, mean fluorescence intensity; NP, nanoparticle; NTA, nanoparticle tracking analysis; PHA, phalloidin; PS, polystyrene; gRNA, single guide RNA.

* Corresponding authors.
E-mail addresses: ester.polo@usc.es (E. Polo), pablo.delpino@usc.es (P. del Pino).

https://doi.org/10.1016/j.jcis.2023.06.015
Received 31 March 2023; Received in revised form 23 May 2023; Accepted 4 June 2023
Available online 7 June 2023

demonstrated nanocarrieŕs fusogenic behavior relies on the fusogen-like properties imparted by the intercalated exogenous lipids, which allows for circumventing lysosomal storage, thereby leading to efficient delivery into the cytosolic milieu where cargo regains function.

1. Introduction

Lipid-derived nanocarriers have shown astonishing performance as drug-delivery systems for manifold diseases [1]. Indeed, the healthcare industry has been seduced by several formulations based on liposomes, leading to medicinal products commonly applied in medical practice [2], mostly as chemotherapeutics or vaccines. We should emphasize the "game changer" role of lipid nanoparticles (NPs) in mRNA-based vaccines during the COVID pandemic and beyond [3,4]. All in all, relatively "simple", cost-effective, self-assembled lipid-based formulations have demonstrated how positively nanomedicines can impact our lives. Many of the advances fueling research on lipid-based nanocarriers rely on synthetic approaches to expand their capabilities beyond mere carriers of lipophilic drugs, including surface engineering ("stealth", stability and targeting properties) [5], lipid cubic phases (high membrane surface area and cargo versatility; that is, cubosomes) [6], and the inclusion of "helper" lipids enabling transfection of non-cell-permeant macromolecules into cells [7,8].

Several groups have developed the field of cell membrane cloaking during the last decade, seeking multifunctional, sustainable, biomimetic approaches for the fabrication of the next generation of lipid-based nanocarriers [9–12]. In brief, cell membrane fragments are isolated from freshly harvested cells (any cell should work for this matter); then, fragments bearing their inherent cell-dependent macromolecular complexity (proteins, lipids, and carbohydrates) are reconstituted to form biomimetic nanocoatings or nanocapsules [13]. Alternatively, glycoproteins isolated from such cell membrane fragments may be anchored on "classic" liposomes [11,14]. Either way, biomimetic cell-derived nanocarriers have shown cell-specific functions derived from the type of cells from which they originated, such as prolonged circulation time, homotypic targeting, and enhanced migration into tumoral sites or inflamed tissue [14–16].

Beyond homing and stealth features, intense synthetic and engineering efforts have been devoted to equipe nanocarriers and therapeutic macromolecules with the capability of surpassing *endo*-lysosomal internalization pathways, as many viruses do, aiming to gain cytosolic delivery of active compounds [17,18]. This challenge remains particularly critical for advanced therapies such as immunotherapy and gene editing, for which dose-efficient and rapid access to specific cytosolic targets go hand in hand with therapeutic effectiveness. Besides physical methods such as electroporation and microinjection, or permeabilization in fixed cells, previous attempts have focused on engineering the nanocarrieŕs surface to achieve direct translocation, to enhance endosomal escape (by endosomolytic lysis, membrane pore formation, proton sponge effect, etc.) or, to bypass endosomal entrapment by inducing fusion of the carrier with the cell membrane [19]. The latest relies on proteins capable of controlling fusion events among cell membranes and pathogens or cell membranes, called fusogens [20] (viral fusogens [18,21] or intracellular fusogens such as SNARE family protein [22,23]).

In this work, we present the design of a fusogenic cell-derived nanocarrier comprising cell membrane extracts and a combination of aromatic labeled and cationic lipids, namely 1,2-dioleoyl-*sn-glycero*-3-phosphoethanolamine labeled with the dye Atto 647 N as aromatic headgroup (DOPE-647 N), and N-[1-(2,3-dioleoyloxy)propyl]-N,N,*N*-trimethylammonium methyl-sulfate (DOTAP). Our modifications were inspired by previous work by A. Csiszár et al. [8,24], aimed at developing fusogenic liposomes by using a specific synergistic combination of lipids, demonstrating the fusogen-like role of cationic lipids with an inverted conical shape and aromatic headgroups. Herein, we adopted this strategy aiming to favor fusion over the otherwise prevalent endocytic pathways typically observed for both solid and soft NPs like liposomes and extracellular vesicles [25]. By modifying the lipid composition of biomimetic vesicles, we aim to engineer nanocarriers with dual functionalities, that is, homotypic targeting capabilities derived from the biomimetic coating and intrinsic fusogenic properties.

2. Results and discussion

2.1. Synthesis and characterization of biomimetic nanocarriers (F)CSMs

The newly developed biomimetic nanocarrier can be efficiently loaded with manifold types of cargo, from small hydrophobic molecules such as the bisbenzimide compound Hoechst H 33258 (HOE) to non-cell-permeant macromolecules such as dextran polymer (DS), the toxin phalloidin (PHA), or a ribonucleoprotein complex (Cas9/sgRNA), or even solid NPs (polystyrene nanoparticles, PSNPs). Upon entering in contact with living cells, in contrast to unmodified cell-derived nanocarriers (herein denoted cellsomes, CSMs), fusogenic cellsomes do not end up in lysosomes. That is, the fusogenic cellsomes (herein referred to as fusosomes, FCSMs), are able to fuse with the cell membrane of living cells, thereby leading to the fast release of the encapsulated compounds into the cytosol of cells, where they regain bioactivity, such as staining intracellular structures (Fig. 1).

CSMs derived from adenocarcinomic human alveolar basal epithelial cells (A549 cells) were produced as previously described elsewhere [26], with minor modifications to encapsulate different types of cargo; details can be found in the Supporting Information (Experimental procedures, **Fig. S1** and **Table S1**). Briefly, cell membrane fragments were extracted from A549 cells. To reconstitute fragments into CSMs, the pellet of harvested membrane fragments was resuspended in phosphate buffered saline (PBS) buffer and subjected to ten consecutive cycles of extrusion through polycarbonate membranes (800 nm pore size). Additionally, the CSM membrane was labeled with a fluorescent membrane lipid-based tracer (DOPE-647 N). Then, FCSMs were produced equivalently, followed by the intercalation of the two lipids (DOPE-647 N/DOTAP, 1/1 mol/mol). Alternatively, in both CSMs and FCSMs, cell membrane extracts were mixed with the target cargo (**Table S1**) and another extrusion cycle was performed. Samples are then purified by spin filters, size exclusion chromatography or centrifugation to remove the free cargo. The size (native number-weighted distribution) and concentration of the CSMs and FCSMs were determined by nanoparticle tracking analysis (NTA) and dynamic light scattering (DLS).

Consistent with previous results [26], DLS measurements showed that the average hydrodynamic diameter of both samples at physiological pH (pH 7.4) remains constant at ~ 200 nm: 217 ± 7 for CSM and 195 ± 26 nm for FCSM (Fig. 2a, **Fig. S2 and Table S2**). Similar results were obtained by electron microscopy analysis (Fig. 2c **and Fig. S3**). NTA analysis of the resulting CSMs and FCSMs showed a mean hydrodynamic diameter of 158 ± 19 and 155 ± 7 nm, respectively (Fig. 2c, **Fig. S4, Table S3**). As expected, also the yield of CSMs and FCSMs is equivalent (**Table S3**), as it depends on the number of cells used per synthesis (10 – 20•10^6 cells); typically, our stocks (1 mL) contain 2 – 3•10^{11} (F)CSM•mL^{-1}. ζ-potential of CSMs and FCSMs are very similar, −24.1 ± 1.0 and −19.3 ± 0.9 mV, respectively (Fig. 2b **and Table S2**); this small difference is compatible with the inclusion of the cationic DOTAP in the case of FCSMs. The positively charge headgroups of the intercalated DOTAP slightly decrease the overall negative charge of the FCMs. That said, in contrast to equivalent fusogenic liposomes with ζ-potential values in the range of 50 mV, [8] both cell-derived nanocarriers are negatively charged. The hydrodynamic size of both CSMs or

FCSMs was not significantly affected by the inclusion of any of the different cargos (**Fig. S4**, **Table S3**), except in the case of PSNPs, in which the system size depends on the NP core diameter (100 nm and 200 nm diameter core NP was chosen as model systems for solid NPs template).

The impact of (F)CSM samples in cell cultures was evaluated. Cellular metabolic activity as an indicator of cell viability was measured by MTT assay to evaluate the possible cytotoxicity effect of the (F)CSM samples. Results shown in Fig. 2d reflected a high cell viability after treatment with several doses of (F)CSM (even up to 500,000 (F)CMS per cell) after 24 h of exposure in A549 cells. In vitro targeting efficacy of (F)CSM was first investigated against different cell lines (tumoral derived cell lines, HeLa and A549 cells, and non-tumoral cell line, MRC-5 fibroblasts). Cancer cell membrane coating has proven its ability for tumor targeting [16,26]. Here, the effect of lipid modification of the fusogenic nanoformulation on its targeting capabilities was also studied by flow cytometry after 10 min and 60 min time of incubation. Higher affinity towards A549 cancer cells than the other cells, such as MRC-5 or HeLa cells, (tumor homing effect *in vitro*) is shown in Fig. 2e for A549 cell-derived (F)CSMs. The biological complexity of the original cell surface and its properties were successfully transferred and retained on the (F)CSM formulation, facilitating the accumulation of the (F)CSMs more efficiently in the cell from the same origin (source). Natural homotypic targeting of CSMs was preserved on FCSMs.

2.2. *Fusogenic properties of (F)CSM nanocarriers*

Then, the fusion capacity of the cell-derived nanocarriers incubated with A549 cells was investigated by live-cell imaging of treated A549 cells using a spinning disk confocal microscopy. Analysis of differences in the fluorescence signal distribution from DOPE-647 N indicates differences in the internalization process of (F)CSMs. A punctuated pattern of fluorescence dots is observed in Fig. 3a, suggesting endosomal localization of CSMs. However, the results in Fig. 3b showing fluorescence signal homogeneously distributed in the cytoplasm and mainly in the membrane of the cells, revealed endosomal escape of FCSMs compared to the cells treated with equivalent doses of non-fusogenic nanocarriers. We also performed Super-Resolution Radial Fluctuations (SRRF) analysis to improve resolution on the confocal images of FCSMs treated cells (Fig. 3b, left panel) [27,28]. SRRF analysis showed the

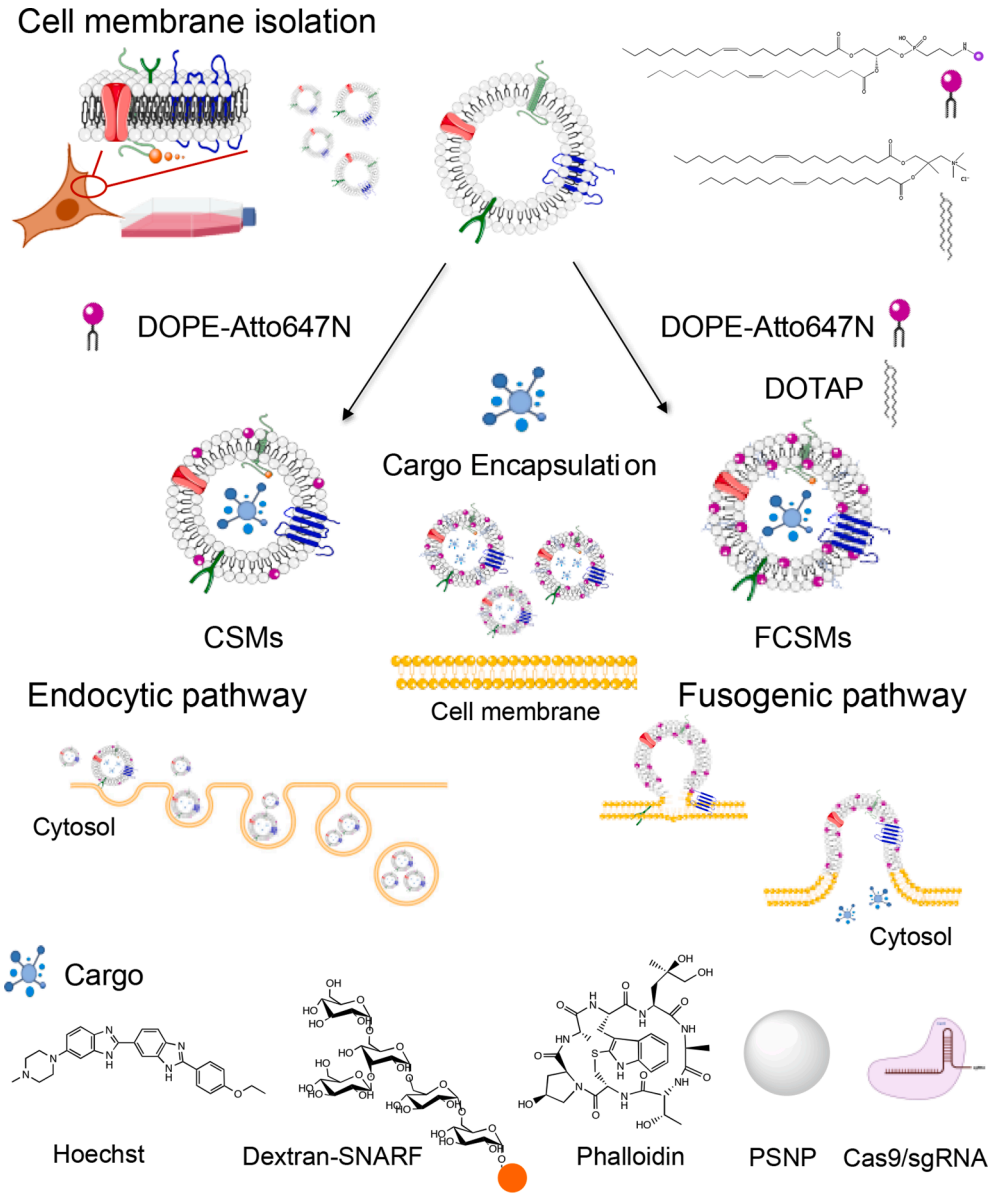

Fig. 1. Schematic representation of CSM vs FCSM formation and their main activity as drug delivery carriers.

DOPE-647 N signal uniformly distributed along the plasmatic cell membrane. Therefore, the intercalation of the lipids DOTAP and DOPE on the CSMs determines the fusogenic properties of FCSMs. We hypothesize that the positive charge introduced by DOTAP allows to increase the electrostatic interaction between the nanocarrier and the negatively charged glycocalyx of the cell membrane; while the presence of a neutral lipid with a cone-like structure such as DOPE assists in membrane destabilization [24,29,30].

To further investigate the difference in the internalization pathway, cellular uptake studies of (F)CSM were examined after blocking all energy-dependent pathways. To assess this, we use temperature control (lowering the temperature to 4 °C) or endocytic inhibitors (a combination of 2-deoxy-D-glucose and sodium azide). Both treatments block all energy-dependent routes [31]. As shown in Fig. 3c, the internalization of CSMs were significantly reduced at 4 °C and by the combination of 2-deoxy-D-glucose and sodium azide, while FCSMs internalization was only minimally reduced after inhibition of the energy-dependent mechanisms. Confocal microscope images also confirm the FCSM fusion with cell membrane at 4 °C (Fig. 3d). That said, the exact fusion mechanism has not been deeply elucidated yet. However, we have demonstrated that by intercalating the cationic and neutral lipids, the fusogenic properties can be incorporated into the intrinsic homotypic targeting capabilities of CSMs without impairing cell viability.

2.3. Intracellular cargo delivery

Next, to investigate the intracellular cargo delivery using FCSMs, we selected different bioactive cargos: from small cell-permeant molecules to non-cell-permeant macromolecules and NPs. The delivery into the cytoplasm of the cells was monitored by confocal microscopy. In all cases, CSMs with encapsulated cargo, and control of non-encapsulated cargo (free) were added to the cells using equivalent cargos concentration. The first selected cargo was the bisbenzimide compound Hoechst H 33258 (HOE), a blue, fluorescent dye typically used for DNA staining in molecular biology; once the sample has been purified by size exclusion chromatography, the cargo loading on (F)CSMs was quantified by fluorescence measurements (**Fig. S5**, **Table S4**). After 10 min incubation with cells, nuclear staining and homogenous plasma membrane staining were observed simultaneously only in cells treated with the FCSM sample (Fig. 4a **left panel,** **Fig. S6-S9**). The fluorescence signal from DOPE-647 N labeled FCSM spread along the cell membrane suggests the membrane fusion between the cell membrane and the nanocarrier. Moreover, the release of HOE inside the cytosol is evidenced by nuclei staining at shorter times (10 min) than achieved with free HOE (**Fig. S6-S7**). As a reference, cells nuclei remained unstained in cells treated with free HOE or CSM@HOE at the same HOE concentration within these time periods. Although the fluorescence signal from DOPE-647 N labeled CSMs appeared punctuated inside the cells, indicating that the CSMs@HOE were successfully internalized by endosomal vesicles, the cargo was not released or leaked into the cytosol after those incubation times (Fig. 4a **right panel**).

Next, a large non-cell-permeant macromolecule was selected as cargo to confirm the intracellular delivery efficacy of FCSMs. Dextran (DS), a hydrophilic polysaccharide of 70 kDa conjugated with fluorescent SNARF dye was encapsulated in (F)CSMs. A549 cells were treated with equivalent concentration of (F)CSMs@DS and free DS. Confocal images after 10 min and 3 h treatment with FCSM@DS show the DS signal homogeneously distributed inside the cytosol of the cells (Fig. 4b **left panel,** **Fig. S10-S14**). In contrast, colocalization between the DS fluorescence signal and DOPE-647 N fluorescence signal from CSM@DS sample was observed, indicating that DS remains encapsulated inside CSMs entrapped in endocytic vesicles (Fig. 4b **right panel,** **Fig. S10-**

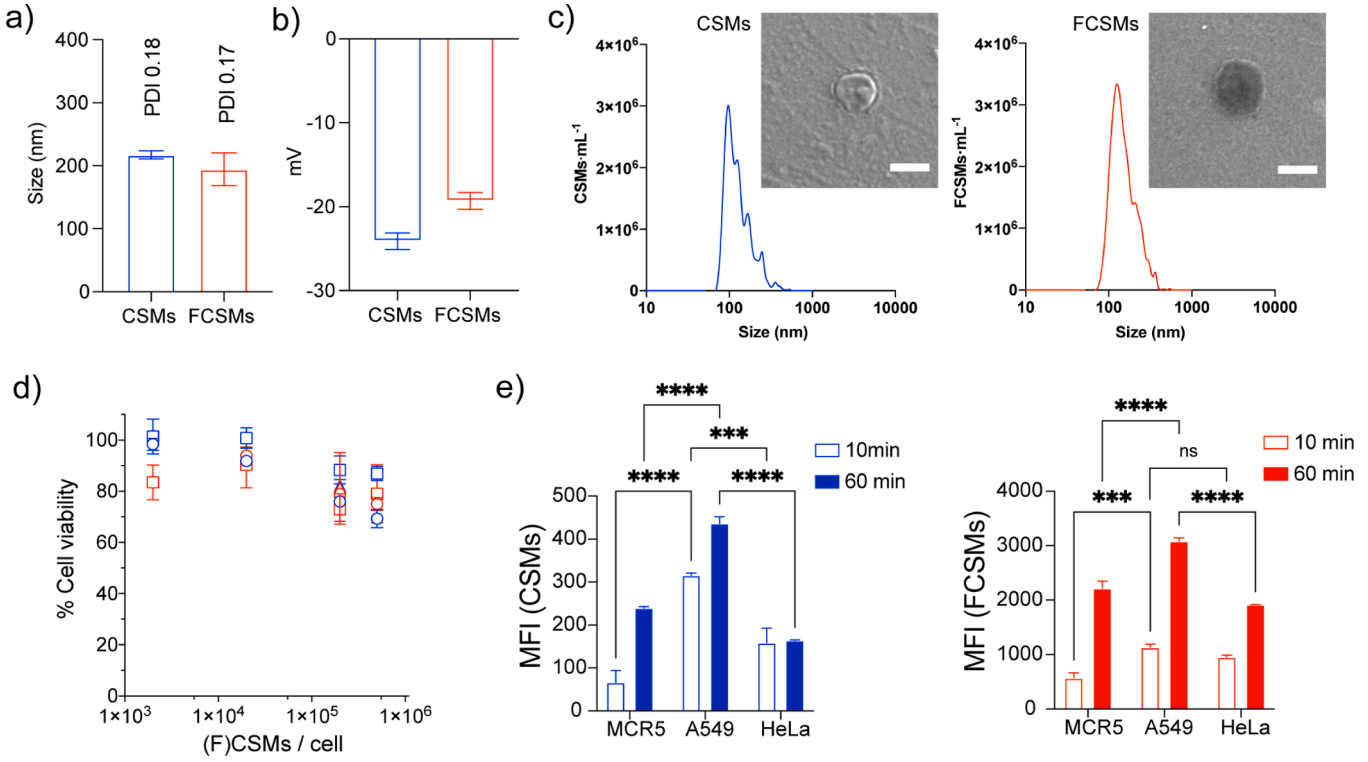

Fig. 2. Characterization of (F)CSM nanocarriers. a) Hydrodynamic size of CSM (blue line) and FCSM (red line) at pH 7.4 analyzed by DLS (n = 3 + SD). (b) ζ-potential of CSM (blue line) and FCSM (red line) analyzed by DLS (n = 3 + SD). c) Size distribution analysis of CSMs (blue line) and FCSMs (red line) by NTA. Scanning electron images of (F)CSMs stained with 2 % of uranyl acetate solution (left). Scale bars: 200 nm. d) Cell viability analysis by MTT assay of A549 cells treated with different concentrations of CSMs (in blue) and FCSMs (in red) for 10 min (squares), 3 h (circles) and 24 h (triangles). (e) Flow cytometric analysis of A549, MRC5, and HeLa cells incubated with CSMs (blue) and FCSMs (red). Mean Fluorescence Intensity (MFI) of DOPE-Atto647 labeled (F)CSMs internalized by cells expressed as mean ± SD, n = 3. Statistical analysis was assessed by two-way ANOVA test (***p = 0.0003, ****p < 0.0001).

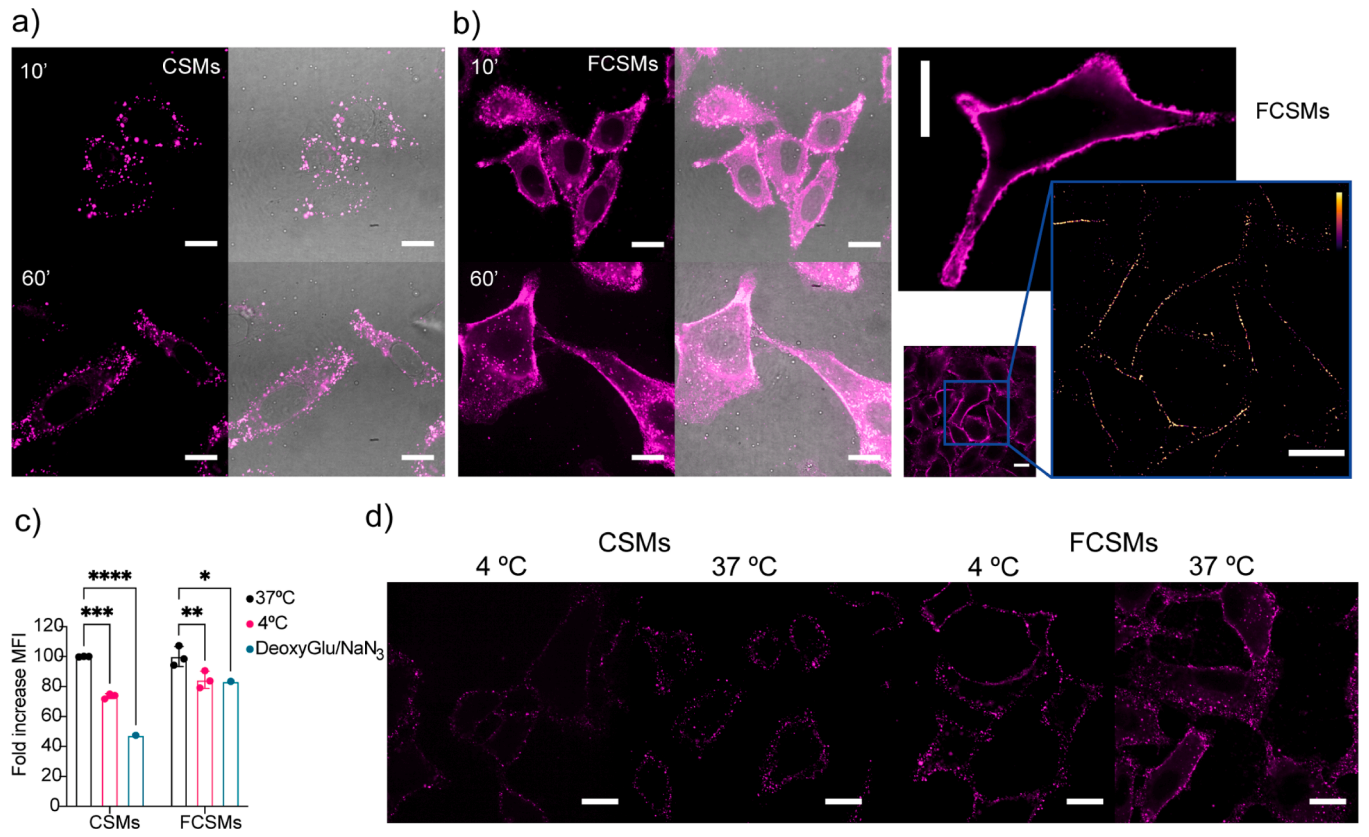

Fig. 3. Confocal images of A549 cells incubated with CSMs (a) and FCSMs (b) for 10 min and 60 min. Fluorescence signal from DOPE-Atto647 (left panel) and brightfield channel merged with the fluorescence channel (right panel). Image of FCSM sample analyzed by the Super-Resolution Radial Fluctuantions (SRRF) algorithm[27] (in blue square). Scale bar: 20 μm. c) (F)CSM uptake in A549 cells at 37 °C, 4 °C and in presence of 2 deoxy-D-glucose and sodium azide. Normalized MFI of DOPE-Atto647 labeled (F)CSMs internalized by cells expressed as mean ± SD, n = 3. Statistical analysis was assessed by two-way ANOVA test (*p = 0.0298, **p = 0.0067, ***p = 0.0002, ****p < 0.0001). d) Confocal images of A549 cells incubated with CSM@DOPE-647 N (left) and FCSM@DOPE-647 N (right) at 37 °C and 4 °C.

S14). A comparative quantitative analysis of the fluorescence staining, evaluated by corrected total cell fluorescence (CTCF) per cell, confirmed that efficient cytosolic cargo release is achieved for both samples, FCSM@HOE (Fig. 4c) and FCSM@DS (Fig. 4d) at 10 min and 3 h. Then, specific binding to an intracellular target was also explored by using the bicyclic heptapeptide phalloidin (PHA) as cargo, a non-cell-permeant toxin used to visualize the F-actin of eukaryotic cells. Free PHA is not capable of crossing the cellular membrane unless cells are permeabilized. Confocal images confirmed the labeling of F-actin of living cells by the intracellular delivery of FITC-labeled PHA from FCSMs after 30 min of treatment (Fig. 4e **and Fig. S14-S15**).

As a proof of concept of the FCSM carriers versatility for cytosolic delivery, solid PSNPs were selected as cargo for their well-documented endocytic efficiency [32]. Overcoming the limitations regarding NP delivery at the intracellular level, while avoiding lysosomal storage and degradation, is one of the main challenges for next-generation nanomedicines. Here we investigate the intracellular delivery of 100 nm and 200 nm sized PSNPs cloaked with (F)CSMs. The interaction between polymeric NPs and cells has been widely studied [33,34]. Besides cellular uptake of NPs depends on NP properties such as size, shape, and surface chemistry, or cellular type [35,36]; energy-dependent endocytic processes are responsible for NP uptake in non-phagocytic cells [32]. 100 nm and 200 nm-sized PSNPs were coated with DOPE-647 N functionalized CSMs and FCSMs. Prior incubation with cells, purified (F)CSM@PSNPs were characterized by NTA (Fig. 5a, **Fig. S4 and Table S3**) and by flow cytometry to validate effective biomimetic coating of PSNPs (Fig. 5b **and Fig. S16**). Then, 200 nm-sized PSNPs and PSNPs cloaked with (F)CSMs were incubated with A549 cells at similar NP dose for 2 h. Confocal images revealed that the fluorescence signal from PSNPs was partly distributed inside the cytosol of the cells treated with the FCSM@PSNP sample (Fig. 5c, **Fig. S17a**). In contrast, fluorescence of PSNP appeared punctuated in the cells treated with CSM@PSNPs (**Fig. S17b**) and with bare PSNPs (**Fig. S17c**), suggesting endosome/lysosome accumulation. Similar results were obtained from 100 nm-sized PSNP cloaked with (F)CSMs (Fig. 5d **and Fig. S18**). In both cases, CSMs coating increased the PSNP uptake rate compared to bare PSNPs. Meanwhile, FCSMs coating also increased the PSNP uptake rate compared to both PSNP with and without CSM coating, while permitted PSNP endosomal escape.

Finally, we applied our FCSMs nanocarriers for the delivery of a CRISPR-associated protein 9 (Cas9) and a single guide RNA (gRNA) against a target gene. The ribonucleoprotein complex (Cas9/sgRNA) enables the manipulation of DNA sequences of cells and organisms, therefore they need to be released in the cytosol and driven to the nucleus to perform gene editing at a specific DNA sequence guided by the sgRNA [37,38]. Viral vectors and lipid-based NPs have been applied for the *in vitro* and *in vivo* delivery of the ribonucleoprotein complex, however, obstacles such as safety, the large size of Cas9, off-target, and low gene editing efficiency still need to be overcome by novel advanced nanocarrieŕs formulations [39,40]. In this work, we used 293-*T*-HEK-dEGFP reporter cells to evaluate the nuclease activity of the ribonucleoprotein complex (Cas9/sgRNA) delivered by the FCSM nanocarriers (Fig. 5e). FCSM which co-encapsulated Cas9/sgRNA complex was analyzed by NTA (**see Fig. S4 and Table S3**) and the fusogenic properties were observed after 10 min of incubation with 293-*T*-HEK-dEGFP expressed cells (**Fig. S19**). We analyzed the Cas9-gRNA gene editing efficiency by quantifying the loss of GFP expression in HEK-dEGFP reporter cells by flow cytometry. As shown in Fig. 5f, the FCSM-mediated

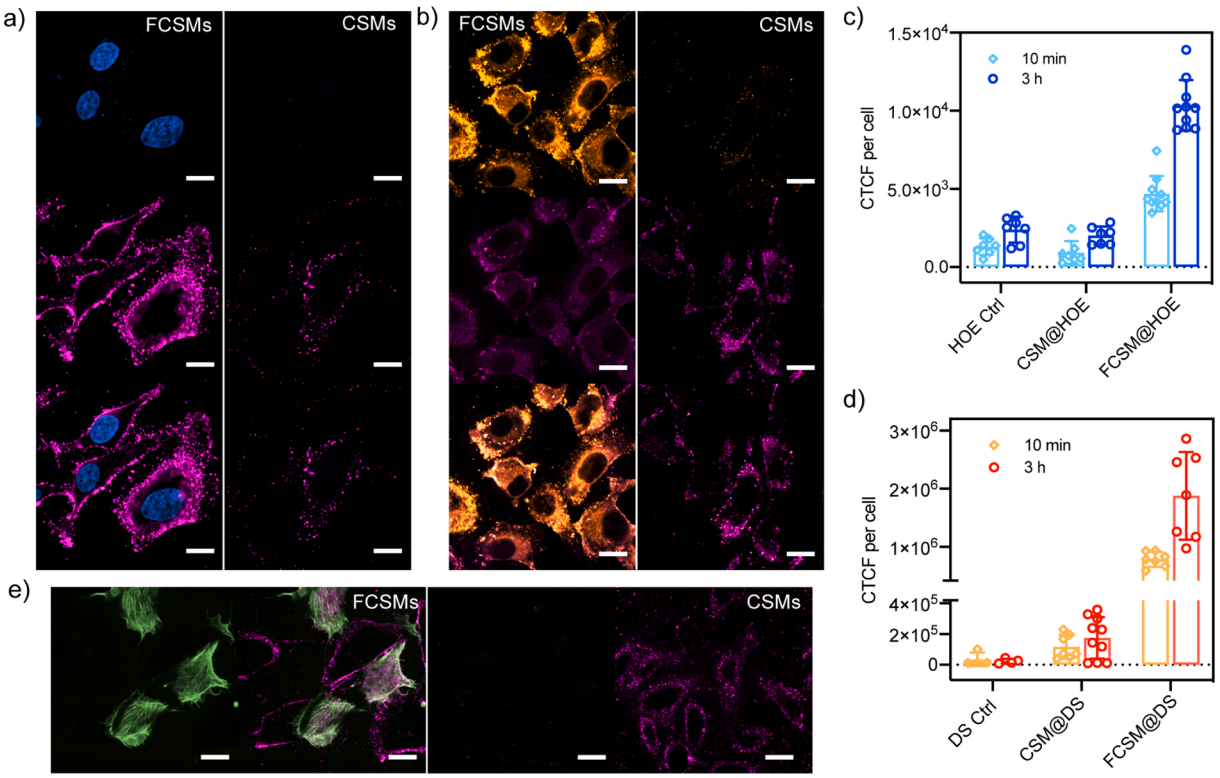

Fig. 4. Cargo delivery inside the cytosol of A549 cells treated with (F)CSMs. a) Confocal images of A549 cells incubated with FCSM@HOE (left panel) or CSM@HOE (right panel) for 10 min. For each panel column, from top to bottom, images show the fluorescence signal from HOE (blue), the fluorescence signal from DOPE-647 N labeled (F)CSM (violet), and the overlay of the two fluorescence channels. Scale bars: 20 μm. b) Confocal images of A549 cells incubated with FCSM@DS (left panel) or CSM@DS (right panel) for 10 min. For each panel column, from top to bottom, images show the fluorescence signal from DS (orange), the fluorescence signal from DOPE-647 N labeled (F)CSM (violet), and the overlay of the two fluorescence channels. Scale bars: 20 μm. c) Comparison of the intracellular fluorescence signal by analyzing corrected total cell fluorescence (CTCF) per cell generated by FCSM@HOE, CSM@HOE, and HOE for 10 min and 3 h of treatment. d) Comparison of the intracellular fluorescence signal by analyzing CTCF per cell generated by FCSM@DS, CSM@DS, and DS for 10 min and 3 h of treatment. e) Confocal images of A549 cells incubated with FCSM@PHA (left panel) or CSM@PHA (right panel) for 30 min (PHA in green and (F)CSM in violet). Scale bars: 20 μm.

CRISPR/Cas9 delivery system yields a reduction down to 35 % of GFP expression in HEK cells after a 12 h single dose administration.

3. Conclusion

In conclusion, in this work we provide a straightforward strategy for intracellular cargo delivery based on the intrinsic abilities of lipid-engineered cancer cell-derived nanocarriers to directly fuse with the plasma membrane and independently of the cargo nature. We achieved intracellular localization of several types of payloads (from small molecules to large non-cell-permeant macromolecules and solid NPs) by combining the nanocarrier biomimetic features (natural homotypic targeting) and fusogenic properties. The underlying mechanism associated with the fusion process and trafficking remains to be elucidated in future studies.

4. Methods

4.1. Synthesis of biomimetic nanoparticles (CSM and FCSMs)

The synthesis of cellsomes (CSMs) was carried out following the protocol described in the literature [26], with a procedure to obtain monodispersed vesicles of 200 nm in size. Synthesized CSMs were derived from 3 different cell lines (tumoral cell lines such as cervix epithelial carcinoma cells, HeLa cells; and adenocarcinomic human alveolar basal epithelial cells, A549 cells). To prepare the CSMs, cells were incubated in 75 cm^2 or 175 cm^2 cell culture flasks in complete Dulbeccós Modified Eagle Medium (DMEM), supplemented with 10 % fetal bovine serum (FBS) and Penicillin-Streptomycin in a humidified chamber at 37 °C under 5 % CO_2. Then, the cells were harvested after trypsinization for 2 min with 2 mL of 0.25 % Trypsin–EDTA. 10 mL of complete DMEM was added to recover the cells and transferred to a 50 mL sterile tube. The cells were collected after centrifugation at 500 g for 5 min. The collected cells (10–20 · 10^6 cells) were washed with phosphate-buffered saline (PBS, pH 7.4) and centrifuged at 600 g for 5 min. The cell pellet was re-suspended in 10 mL of hypotonic buffer (0.25X PBS) containing 1X Protease inhibitor cocktail and incubated in an ice bath for 10 min. Then the cell lysis was carried out by 4 cycles of freezing in liquid nitrogen for 1 min followed by thawing at 37 °C for 10 min. Finally, the solution was placed in a bath sonicator for 5 min. To purify the cell membrane fragments, the solution was subjected to several centrifugation steps. First the solution was centrifuged at 700 g for 10 min at 4 °C to discard nuclei or whole cells. Then the cell membrane fragments that remained in the supernatant were precipitated by centrifugation at 15,000 g for 30 min at 4 °C. The pellet was dispersed in 1 mL of 20 mM of 2-(4-(2-hydroxyethyl)-1-piperazinyl)-ethanesulfonic acid (HEPES, pH 7.4) buffer and subjected to 10 cycles of extrusion by using an Avanti® Mini extruder with a 800 nm polycarbonate membrane. Fluorescently labeled CSMs were produced using a fluorescent phospholipid (DOPE-Atto647N, 18:1 (Δ9-Cis) PE, 1,2-Dioleoyl-*sn-glycero*-3-phosphoethanolamine labeled with Atto647N) that was added to the lipid bilayer of the CSMs. 1 mL of obtained CSMs dispersed in PBS were mixed with the 2 μL of 1 $mg{\cdot}mL^{-1}$ of DOPE-Atto647N and sonicated for 10 min. The resulting CSMs were extruded 10 cycles using an Avanti® Mini extruder (with an 800 nm polycarbonate membrane), purified by ultrafiltration using Amicon® Ultra-0.5 Centrifugal Filter Devices (cut-off of 100 kDa) and washed with 20 mM HEPES at least 3 times.

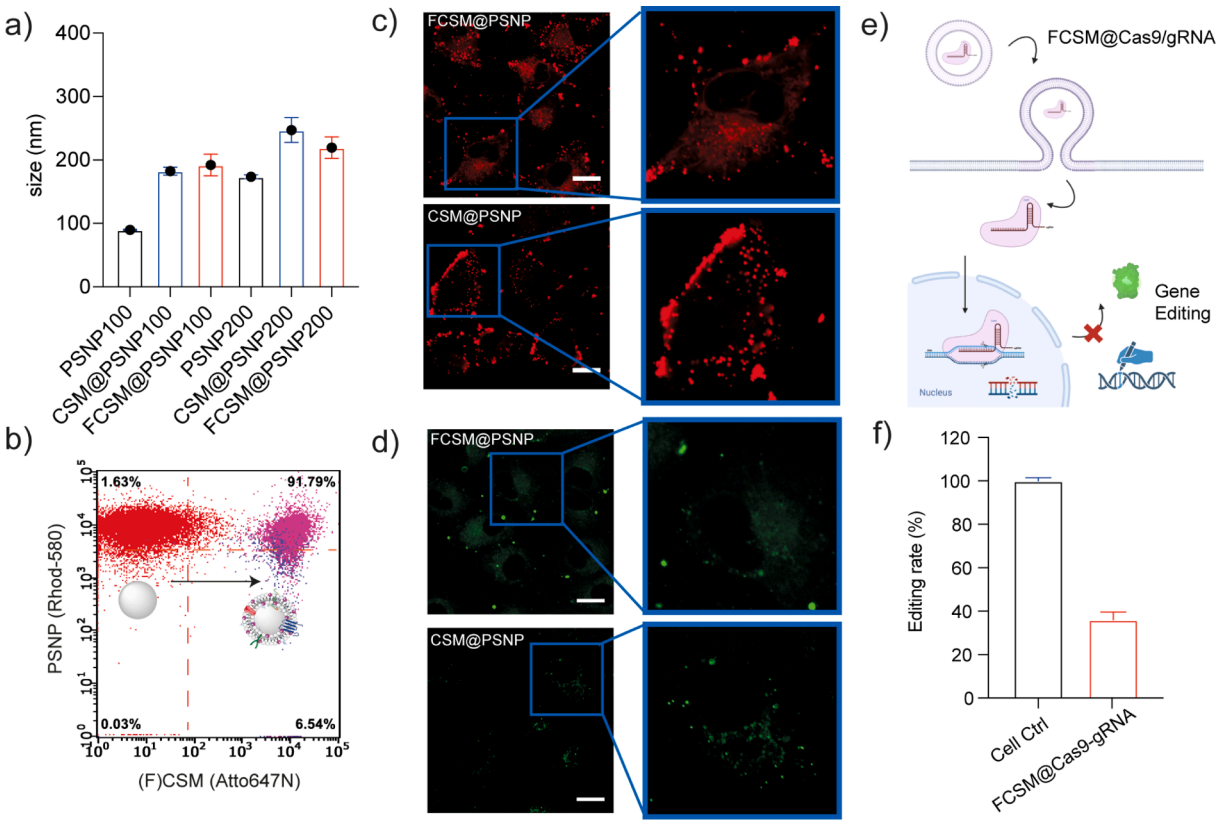

Fig. 5. A) hydrodynamic size of PSNPs (black line), CSM coated PSNPs (blue line) and FCSM coated PSNP (red line) at ph 7.4 analyzed by dls (n = 3 + SD). b) Characterization of (F)CSM cloaked PSNP by flow cytometry: scatter density plots of Rhodamine fluorescence channel (corresponding to PSNPs signal) versus Atto647N fluorescence channel (corresponding to (F)CSMs signal) for PSNP sample and (F)CSM@PSNP sample. c) and d) Confocal images of A549 cells incubated with (F)CSM@PSNP for 2 h (200 nm sized PSNP in red (c) and 100 nm PSNP in green (d)). Scale bars: 20 μm. e) Schematic representation of CRISPR/Cas9 gene editing delivered by FCSMs. f) Percentage of editing rate of dEGFP expression in HEK-293 before and after FCSM@Cas9-gRNA treatment: HEK cells were treated with FCSM@Cas9-gRNA for 12 h, and GFP expression in cells was analyzed by flow cytometer after 48 h (n = 3 + SD).

Fusogenic cellsomes (FCSMs) were prepared using lipid components like neutral lipids, positively charged lipids and aromatic/fluorescent compounds. Precisely, 1 mL of non-fluorescent CSMs (1 mg) dispersed in 20 mM HEPES was mixed with 20 μL of DOPE-Atto647N (1 mg·mL^{-1}) and 10 μL of 18:1 TAP 1,2-dioleoyl-3-trimethylammonium-propane, DOTAP (1 mg·mL^{-1}). The solution was sonicated for 10 min and extruded 10 cycles using an Avanti® Mini extruder with an 800 nm polycarbonate membrane and purified by ultrafiltration using Amicon® Ultra-0.5 Centrifugal Filter Devices (cut-off of 100 KDa) and washing the solution with 20 mM HEPES at least 3 times.

4.2. CSM and FCSM cargo loading

To incorporate the corresponding cargo (Hoechst, Dextran-SNARF, Phalloidin-FITC, PS NPs, Cas9/sgRNA) to the (F)CSMs, the corresponding volume of the specific cargo (Table S1) was added to the (F)CSMs solutions. The cargo/(F)CSMs solution was stirred for 10 min and sonicated for 5 min at RT. The resulting (F)CSMs were extruded 10 cycles using an Avanti® Mini extruder with a 800 nm polycarbonate membrane. The (F)CSMs@cargo sample was purified from the excess of non-incorporated cargo molecules by size exclusion chromatography, ultrafiltration by using Amicon® Ultra-0.5 Centrifugal Filter Devices (cut-off of 100 kDa), or by centrifugation (see Supplementary Information). The samples were concentrated/resuspended in 100 μL 20 mM HEPES volume. The amount of cargo molecules loaded into the (F)CSMs was quantified by fluorescence analyses using a Microplate reader (TECAN, Infinite® 200 PRO) equipped with monochromator-based optics and wavelength selection between 280 and 850 nm.

4.3. Characterization of CSM and FCSM.

(F)CSM samples were characterized by dynamic light scattering (DLS), nanoparticle tracking analysis (NTA) and scanning electron microscopy (SEM). All the samples were analysed in PBS or in 20 mM HEPES buffer pH 7.4 by using a DLS Malvern Zetasizer Nano ZSP (Malvern Instrument ltd.). All measurements were carried out at 37 °C. All the samples were analysed by using a NanoSight NS300 (Malvern Instrument ltd.) equipped with a 405 nm laser. All measurements were carried out at 24 °C. (F)CSMs were diluted 1:10,000 in MilliQ water (200 nm filtered) to a final volume of 1 mL and loaded in the measurement chamber with a flow rate of 50 mL/min. For SEM analysis, (F)CSMs samples were stained by using a 2 % Uranile acetate solution. 2 μL of (F)CSMs suspension was deposited onto the a 3 – 4 nm thick film of amorphous carbon supported on a 400 mesh copper grid (Ted Pella Inc., #01822-F). All images in this section were obtained using a scanning electron microscope ZEISS FESEM ULTRA Plus.

4.4. Cellular uptake

HeLa, A549 and human lung fibroblast MRC-5 cell lines were cultured in complete media (DMEM supplemented with 10 % FBS and 1 % P/S). Cells were maintained under humid conditions at 37 °C and 5 % of CO_2. Cells were seeded in 48-well plate at a density of 25,000 cells per well in 0.3 mL of complete media. After 24 h, the cell medium was replaced with the freshly prepared DOPE-Atto647N labeled CSMs or FCSMs dispersions. Homotypic experiments were performed by exposing the cells to (F)CSM dispersions at 37 °C and 5 % CO_2 for 10 min in PBS and 1 h in complete media. After (F)CSMs exposure, cells were

washed with 0.3 mL PBS per well. Then, cells were harvested after trypsinization for 2 min with 0.075 mL 0.25 % Trypsin–EDTA. 0.15 mL of PBS or complete media was added to each well to recover the cells. Cells were pelleted by centrifugation at 300 g for 3 min, then resuspended in 200 μL of cell media or PBS. Cell fluorescence intensity was measured using a Guava Millipore flow cytometer equipped with 642 nm red laser (Cat. No. A16501, A16504) coupled with 620/50 nm filter. Results are reported as the median of cell fluorescence intensity.

4.5. Cytotoxicity assay

In order to study the number of viable cells after (F)CSMs exposure, 3-[4,5-dimethylthiazol-2-yl]-2,5-diphenyltetrazolium bromide (MTT) assay was performed. A549 cells were seeded in 96-well plates, 7,500 cells per well in 100 μL of cell growth medium 24 h before (F)CSMs exposure. The media was then removed and 100 μL of cell culture growth medium with the desired concentration of (F)CSMs were added. After different incubation times (10 min, 3 h and 24 h), each well was rinsed once with PBS and 110 μL of freshly prepared MTT solution diluted in cDMEM was added. After 3 h at 37 °C and 5 % CO_2, 85 μL of MTT solution were removed, 50 μL of DMSO were added to each well to dissolve the formazan crystals and the 96-well plate was left for 10 min at 37 °C and 5 % CO_2. Then, absorbance was measured with a plate reader (TECAN, Infinite® 200 PRO) at 540 nm.

4.6. In vitro cargo release inside living cells by confocal microscopy

Cells were seeded in a μ-Slide VI 0.4 (#80606) well plate at a concentration of 15,000 cells per well. Cells were allowed to grow in complete media at 37 °C and 5 % CO_2 for 24 h to reach 70 % of confluence. The (F)CSMs samples were exposed to the cells at different time treatments (10 min in PBS and 1 h in complete media, at 37 °C and 5 % CO_2) at HOE, DS and PHA concentrations of 3.3 μM, 70 nM and 0.2 μM, respectively. The (F)CSMs@PSNPs samples were added to the cells at the concentration of 12,000 NPs/cell. Cells were washed twice with fresh PBS and complete media without phenol red was added. Confocal images were captured on an Andor Dragonfly spinning disk confocal system mounted on a Nikon TiE microscope equipped with a Zyla 4.2 PLUS camera (Andor, Oxford Instruments) and an OKO-lab incubator to keep cells at 37 °C during the whole experiment. The samples were excited with four different lasers (405, 488, 561 and 637 nm lasers) and the emitted fluorescence was collected by the filter wheel (450/50 nm, 525/50 nm, 620/50 nm and 725/40 nm) with appropriate combinations of them. Images were taken with different magnification objectives (20X, 100X). All the images were processed with ImageJ®.

4.7. Cas9/gRNA intracellular delivery

293-*T*-HEK-dEGFP cells were seeded in 96-well plate at a density of 18,000 cells per well in 0.1 mL of cDMEM. After 24 h, cells were washed with PBS and the medium was replaced with freshly prepared 0.01 mL of FCSM@Cas9-gRNA in 0.09 mL of cDMEM. Experiments were performed by exposing the cells to Cas9-gRNA dispersions at a ratio of 50 ng:10 ng (Cas9:gRNA) per well. After 12 h, cells were washed with PBS, and the medium was replaced with freshly complete DMEM. Then 36 h after, cells were washed with PBS and were harvested after trypsinization for 2 min with 0.03 mL 0.25 % Trypsin-EDTA. 0.12 mL of PBS was added to each well to dilute Trypsin-EDTA concentration. Cell fluorescence intensity was measured using a Guava Millipore flow cytometer.

Declaration of Competing Interest

The authors declare that they have no known competing financial interests or personal relationships that could have appeared to influence the work reported in this paper.

Data availability

Data will be made available on request.

Acknowledgment

The authors thank the financial support of the European Research Council (starting grant #950421), the European Union (INTERREG V-A Spain–Portugal #0624_2IQBIONEURO_6_E, NextGenerationEU/PRTR and ERDF), the MCIN/AEI (PID2020-119206RB-I00, PID2020-119479RA-I00, PID2019-111218RB-I00, RYC-2017-23457 and RYC-2019-028238-I), and the Xunta de Galicia (ED431F 2021/02, 2021-CP090, ED431C 2022/018, and Centro Singular De Investigación de Galicia Accreditation 2019–2022 #ED431G 2019/03). This project was also supported by the ISCIII, under the framework of EuroNanoMed III_2020 (AC20/00041, PLATMED). We would also like to thank our colleagues Dr. M. Collado and Dr. M.A. Moreno-Mateos for their valuable insights and suggestions. We thank Dr. M. Collado (IDIS, Spain) for a gift of 293-T-HEK-dEGFP cells.

Appendix A. Supplementary data

Supplementary data to this article can be found online at https://doi.org/10.1016/j.jcis.2023.06.015.

References

[1] R. Tenchov, R. Bird, A.E. Curtze, Q. Zhou, Lipid Nanoparticles—From Liposomes to mRNA Vaccine Delivery, a Landscape of Research Diversity and Advancement, ACS Nano 15 (2021) 16982–17015.
[2] D.E. Large, R.G. Abdelmessih, E.A. Fink, D.T. Auguste, Liposome composition in drug delivery design, synthesis, characterization, and clinical application, Adv. Drug Del. Rev. 176 (2021), 113851.
[3] A. Hussain, H. Yang, M. Zhang, Q. Liu, G. Alotaibi, M. Irfan, H. He, J. Chang, X.-J. Liang, Y. Weng, Y. Huang, mRNA vaccines for COVID-19 and diverse diseases, J. Control. Release 345 (2022) 314–333.
[4] R. Verbeke, I. Lentacker, S.C. De Smedt, H. Dewitte, The dawn of mRNA vaccines: The COVID-19 case, J. Control. Release 333 (2021) 511–520.
[5] Y. Xu, T. Fourniols, Y. Labrak, V. Préat, A. Beloqui, A. des Rieux, Surface Modification of Lipid-Based Nanoparticles, ACS Nano 16 (2022) 7168–7196.
[6] H.M.G. Barriga, M.N. Holme, M.M. Stevens, Cubosomes: The Next Generation of Smart Lipid Nanoparticles? Angew. Chem. Int. Ed. 58 (2019) 2958–2978.
[7] S. Kube, N. Hersch, E. Naumovska, T. Gensch, J. Hendriks, A. Franzen, L. Landvogt, J.-P. Siebrasse, U. Kubitscheck, B. Hoffmann, R. Merkel, A. Csiszár, Fusogenic Liposomes as Nanocarriers for the Delivery of Intracellular Proteins, Langmuir 33 (2017) 1051–1059.
[8] R. Kolašinac, C. Kleusch, T. Braun, R. Merkel, A. Csiszár, Deciphering the Functional Composition of Fusogenic Liposomes, Int. J. Mol. Sci. 19 (2018) 346.
[9] R.H. Fang, A.V. Kroll, W. Gao, L. Zhang, Cell Membrane Coating Nanotechnology, Adv. Mater. 30 (2018) 1706759.
[10] C.-M.-J. Hu, R.H. Fang, K.-C. Wang, B.T. Luk, S. Thamphiwatana, D. Dehaini, P. Nguyen, P. Angsantikul, C.H. Wen, A.V. Kroll, C. Carpenter, M. Ramesh, V. Qu, S.H. Patel, J. Zhu, W. Shi, F.M. Hofman, T.C. Chen, W. Gao, K. Zhang, S. Chien, L. Zhang, Nanoparticle biointerfacing by platelet membrane cloaking, Nature 526 (2015) 118–121.
[11] A. Parodi, N. Quattrocchi, A.L. van de Ven, C. Chiappini, M. Evangelopoulos, J. O. Martinez, B.S. Brown, S.Z. Khaled, I.K. Yazdi, M.V. Enzo, L. Isenhart, M. Ferrari, E. Tasciotti, Synthetic nanoparticles functionalized with biomimetic leukocyte membranes possess cell-like functions, Nat. Nanotechnol. 8 (2013) 61–68.
[12] L. Shi, J. Zhang, M. Zhao, S. Tang, X. Cheng, W. Zhang, W. Li, X. Liu, H. Peng, Q. Wang, Effects of polyethylene glycol on the surface of nanoparticles for targeted drug delivery, Nanoscale 13 (2021) 10748–10764.
[13] V. Chugh, K. Vijaya Krishna, A. Pandit, Cell Membrane-Coated Mimics: A Methodological Approach for Fabrication, Characterization for Therapeutic Applications, and Challenges for Clinical Translation, ACS Nano 15 (2021) 17080–17123.
[14] R. Molinaro, C. Corbo, J.O. Martinez, F. Taraballi, M. Evangelopoulos, S. Minardi, I.K. Yazdi, P. Zhao, E. De Rosa, M.B. Sherman, A. De Vita, N.E. Toledano Furman, X. Wang, A. Parodi, E. Tasciotti, Biomimetic proteolipid vesicles for targeting inflamed tissues, Nat. Mater. 15 (2016) 1037–1046.
[15] C.-M.-J. Hu, L. Zhang, S. Aryal, C. Cheung, R.H. Fang, L. Zhang, Erythrocyte membrane-camouflaged polymeric nanoparticles as a biomimetic delivery platform, PNAS 108 (2011) 10980–10985.
[16] J.-Y. Zhu, D.-W. Zheng, M.-K. Zhang, W.-Y. Yu, W.-X. Qiu, J.-J. Hu, J. Feng, X.-Z. Zhang, Preferential Cancer Cell Self-Recognition and Tumor Self-Targeting by Coating Nanoparticles with Homotypic Cancer Cell Membranes, Nano Lett. 16 (2016) 5895–5901.

[17] A. Barba-Bon, G. Salluce, I. Lostalé-Seijo, K.I. Assaf, A. Hennig, J. Montenegro, W. M. Nau, Boron clusters as broadband membrane carriers, Nature 603 (2022) 637–642.
[18] J.H. Park, A. Mohapatra, J. Zhou, M. Holay, N. Krishnan, W. Gao, R.H. Fang, L. Zhang, Virus-Mimicking Cell Membrane-Coated Nanoparticles for Cytosolic Delivery of mRNA, Angew. Chem. Int. Ed. 61 (2022) e202113671.
[19] W. He, X. Xing, X. Wang, D. Wu, W. Wu, J. Guo, S. Mitragotri, Nanocarrier-Mediated Cytosolic Delivery of Biopharmaceuticals, Adv. Funct. Mater. 30 (2020) 1910566.
[20] N. Segev, O. Avinoam, B. Podbilewicz, Fusogens, Curr. Biol. 28 (2018) R378–R380.
[21] F.A. Rey, S.-M. Lok, Common Features of Enveloped Viruses and Implications for Immunogen Design for Next-Generation Vaccines, Cell 172 (2018) 1319–1334.
[22] G.A. Daudey, M. Shen, A. Singhal, P. van der Est, G.J.A. Sevink, A.L. Boyle, A. Kros, Liposome fusion with orthogonal coiled coil peptides as fusogens: the efficacy of roleplaying peptides, Chem. Sci. 12 (2021) 13782–13792.
[23] Y. Yang, N.N. Margam, Structural Insights into Membrane Fusion Mediated by Convergent Small Fusogens, Cells 10 (2021) 160.
[24] A. Csiszár, N. Hersch, S. Dieluweit, R. Biehl, R. Merkel, B. Hoffmann, Novel Fusogenic Liposomes for Fluorescent Cell Labeling and Membrane Modification, Bioconjug. Chem. 21 (2010) 537–543.
[25] B.S. Joshi, M.A. de Beer, B.N.G. Giepmans, I.S. Zuhorn, Endocytosis of Extracellular Vesicles and Release of Their Cargo from Endosomes, ACS Nano 14 (2020) 4444–4455.
[26] E. Soprano, A. Alvarez, B. Pelaz, P. del Pino, E. Polo, Plasmonic Cell-Derived Nanocomposites for Light-Controlled Cargo Release inside Living Cells, Adv. Biosyst. 4 (2020) 1900260.
[27] S. Culley, K.L. Tosheva, P. Matos Pereira, R. Henriques, SRRF: Universal live-cell super-resolution microscopy, Int. J. Biochem. Cell Biol. 101 (2018) 74–79.
[28] N. Gustafsson, S. Culley, G. Ashdown, D.M. Owen, P.M. Pereira, R. Henriques, Fast live-cell conventional fluorophore nanoscopy with ImageJ through super-resolution radial fluctuations, Nat. Commun. 7 (2016) 12471.
[29] D. Simberg, S. Weisman, Y. Talmon, Y. Barenholz, DOTAP (and other cationic lipids): chemistry, biophysics, and transfection, Crit. Rev. Ther. Drug Carrier Syst. 21 (2004) 257–317.
[30] A. Joardar, G.P. Pattnaik, H. Chakraborty, Mechanism of Membrane Fusion: Interplay of Lipid and Peptide, J. Membr. Biol. 255 (2022) 211–224.
[31] J.J. Rennick, A.P.R. Johnston, R.G. Parton, Key principles and methods for studying the endocytosis of biological and nanoparticle therapeutics, Nat. Nanotechnol. 16 (2021) 266–276.
[32] T. dos Santos, J. Varela, I. Lynch, A. Salvati, K.A. Dawson, Effects of Transport Inhibitors on the Cellular Uptake of Carboxylated Polystyrene Nanoparticles in Different Cell Lines, PLoS One 6 (2011) e24438.
[33] S. Behzadi, V. Serpooshan, W. Tao, M.A. Hamaly, M.Y. Alkawareek, E.C. Dreaden, D. Brown, A.M. Alkilany, O.C. Farokhzad, M. Mahmoudi, Cellular uptake of nanoparticles: journey inside the cell, Chem. Soc. Rev. 46 (2017) 4218–4244.
[34] B. Yameen, W.I. Choi, C. Vilos, A. Swami, J. Shi, O.C. Farokhzad, Insight into nanoparticle cellular uptake and intracellular targeting, J. Control. Release 190 (2014) 485–499.
[35] D. Hühn, K. Kantner, C. Geidel, S. Brandholt, I. De Cock, S.J.H. Soenen, P. Rivera_ Gil, J.-M. Montenegro, K. Braeckmans, K. Müllen, G.U. Nienhaus, M. Klapper, W. J. Parak, Polymer-Coated Nanoparticles Interacting with Proteins and Cells: Focusing on the Sign of the Net Charge, ACS Nano 7 (2013) 3253–3263.
[36] O. Lunov, T. Syrovets, C. Loos, J. Beil, M. Delacher, K. Tron, G.U. Nienhaus, A. Musyanovych, V. Mailänder, K. Landfester, T. Simmet, Differential Uptake of Functionalized Polystyrene Nanoparticles by Human Macrophages and a Monocytic Cell Line, ACS Nano 5 (2011) 1657–1669.
[37] P. Mali, L. Yang, K.M. Esvelt, J. Aach, M. Guell, J.E. DiCarlo, J.E. Norville, G. M. Church, RNA-Guided Human Genome Engineering via Cas9, Science 339 (2013) 823–826.
[38] P.D. Hsu, E.S. Lander, F. Zhang, Development and Applications of CRISPR-Cas9 for Genome Engineering, Cell 157 (2014) 1262–1278.
[39] D. Rosenblum, A. Gutkin, R. Kedmi, S. Ramishetti, N. Veiga, A.M. Jacobi, M. S. Schubert, D. Friedmann-Morvinski, Z.R. Cohen, M.A. Behlke, J. Lieberman, D. Peer, CRISPR-Cas9 genome editing using targeted lipid nanoparticles for cancer therapy, Sci. Adv. 6 (2020) eabc9450.
[40] E. Senís, C. Fatouros, S. Große, E. Wiedtke, D. Niopek, A.-K. Mueller, K. Börner, D. Grimm, CRISPR/Cas9-mediated genome engineering: An adeno-associated viral (AAV) vector toolbox, Biotechnol. J. 9 (2014) 1402–1412.